First-principles molecular dynamics study of the structure and dynamic behavior of liquid $Li_4BN_3H_{10}$

David E. Farrell,* Dongwon Shin, and C. Wolverton†
Department of Materials Science and Engineering, Northwestern University, Evanston, Illinois 60208, USA
(Received 28 September 2009; published 10 December 2009)

We have applied density-functional theory based *ab initio* molecular dynamics to examine $Li_4BN_3H_{10}$ at temperatures both above and below the experimental melting point. We examine the structure of the liquid, diffusivity, vibrational spectra and compare to both experimental data and analogous properties from solid-state calculations. We find the following: (1) the liquid state, like the solid state, is primarily a mixture of Li^+, BH_4^-, and NH_2^- with ionic interactions between the BH_4^- and NH_2^- anions and the Li^+ cations. (2) We observe the reaction of two amide anions exchanging hydrogen to form ammonia and an imide anion: $2NH_2^- \rightarrow NH_3 + NH^{2-}$. (3) The liquid demonstrates wide bond-angle distributions in the BH_4^- and NH_2^- units and thus these anionic units are not simply rigid complexes. (4) The Li^+ sublattice disorders before the anionic sublattices and the liquid exhibits very fast Li^+ diffusion. We calculate the activation energy and pre-exponential factor for Li^+ diffusivity in the liquid to be ~ 20 kJ/mol and 15×10^{-4} cm^2/s, respectively. (5) Finally, we find that the liquid contains the same generic types of vibrational modes as the solid, however the lower-frequency anionic vibration and rotation modes become more prominent with increasing temperature.

DOI: 10.1103/PhysRevB.80.224201 PACS number(s): 61.20.Ja

I. INTRODUCTION

In recent years, numerous research groups have put forth much effort toward the realization of efficient, high-capacity hydrogen storage for hydrogen-based vehicles.[1] One promising class of materials for this application is complex hydrides.[2,3] These materials have the possibility of very high gravimetric and volumetric hydrogen storage densities, making them attractive materials if they can be shown to have high rates of hydrogen desorption and absorption at near-ambient conditions.

One particular complex hydride that has received significant attention due to its high hydrogen storage capacity is the quaternary compound $Li_4BN_3H_{10}$, found to release more than 10 wt % H_2. The hydrogen storage properties and crystal structure of this material was studied experimentally by Pinkerton *et al.*[4] and subsequently by Filinchuk *et al.*[5] and Chater *et al.*[6] These experimental studies prompted several theoretical studies that examined the crystal structure, vibrational spectra and reaction energetics of solid $Li_4BN_3H_{10}$.[7–9] The experimental and theoretical analysis reveal solid $Li_4BN_3H_{10}$ to be an ionic compound consisting of four Li^+ cations, one BH_4^-, and three NH_2^- anionic units per formula unit,[6] whose solid structure has bcc symmetry (space group $I2_13$) and a lattice parameter of roughly 10.6 Å.[8] However, the initial experiments indicated that hydrogen and ammonia release occur at approximately 520 K, above the melting temperature of ~ 460 K,[4,5] though a more recent experimental study of $NiCl_2$ catalyzed $Li_4BN_3H_{10}$ demonstrated hydrogen desorption at approximately 400 K, with no change in the ammonia release temperature.[10] The fact that hydrogen and ammonia release occur near or above the melting point indicates that structural characterization of the *liquid* state is important in understanding the mechanism of hydrogen release from this material. Here, we use first-principles calculations based on density-functional theory (DFT) to elucidate the detailed atomic structure, diffusivity, and vibrational properties of liquid $Li_4BN_3H_{10}$.

DFT-based calculations have been used to predict and explore the ground-state crystal structures, vibrational properties and thermodynamics of a number of hydrides,[11–16] including complex hydrides such as $LiBH_4$,[17] $NaAlH_4$,[18] $LiNH_2$,[19] Li_2NH,[20,21] $Ca(AlH_4)_2$,[22] $Li_2Mg(NH)_2$,[23] and $Ca(BH_4)_2$.[24] Additionally, groups have applied nonzero temperature *ab initio* molecular dynamics (AIMD) to materials such as $NaAlH_4$ (Ref. 25) to explore diffusion in the solid hydride as well as structural and vibrational properties of hydride clusters[26] and to predict solid-state transformations in $LiBH_4$.[27] Molecular dynamics has also been used very recently to investigate the structure and diffusion characteristics in Li_2NH.[28] One advantage of AIMD is the ability to explicitly follow the trajectory of a given atom through time, allowing one to see any diffusion events or chemical reactions as they occur. However, AIMD is generally limited to a small time scale, often shorter than the typical time scale for solid-state diffusion. This time-scale limitation may be partially overcome by studying materials where the phenomenon of interest occurs in the liquid state, such as $Li_4BN_3H_{10}$, because the kinetics are generally much faster than in the solid.

We have used AIMD to examine the structural, vibrational, and diffusion characteristics of liquid $Li_4BN_3H_{10}$ for temperatures from 300 to 2000 K. We find that the liquid state, like the solid state, is a mixture of Li^+, BH_4^-, and NH_2^- with ionic interactions between the BH_4^- and NH_2^- units and the Li^+ ions. However, we show that the BH_4^- and NH_2^- units are not rigid complexes but rather undergo wide bond-angle fluctuations about their ideal positions. Additionally, we see chemical fluctuations take place at temperatures above 600 K. We observe the reaction of two amide anions exchanging hydrogen to form ammonia and an imide anion: $2NH_2^- \rightarrow NH_3 + NH^{2-}$. We also find interesting structural and kinetic properties on the cation sublattice: the Li^+ sublattice disorders before the B, N, and H sublattices, and we find indications of high Li^+ diffusion in the liquid. Finally, we find that

 ©2009 The American Physical Society

the liquid contains the major vibrational modes of the solid, however the low-frequency anion and cation vibration modes become more prominent with increasing temperature.

II. METHODOLOGY

We perform our calculations with the Vienna *ab initio* simulation package [VASP (Refs. 29–33)] plane-wave DFT code. We calculate the interionic forces with high-precision DFT calculations using the Perdew-Wang 1991 generalized gradient approximation (GGA),[34] Blöchl's projector augmented wave (PAW) method[33,35] for core-valence electron interactions, and gamma point only sampling in k space. We employ a Gaussian smearing scheme for the electronic occupancies with a width of 0.1 eV. We choose the "standard" potentials for H, B, and N in VASP and an "s-valent" potential for Li (the so-called "Li sv" potential), with an overall energy cutoff of 500 eV. These parameters are similar to those used in Ref. 8 for the solid state with the only differences being that we use gamma-point sampling and "softer" pseudopotentials.

In order to ensure that gamma-point sampling was sufficient, prior to the calculations for this work, we performed a static minimization on the 144 atom starting structure and compared it to results obtained for the same system with a $2\times2\times2$ Monkhorst-Pack k-point mesh. We found that the gamma-point calculation total energy was converged to within 0.3 meV/atom and the lattice parameter to within 0.002 Å. We also compared to the "hard" VASP PAW/GGA potentials like those used in Ref. 8 (also with gamma-point sampling) and found the lattice parameter was converged to within 0.004 Å. We judged these to be sufficiently small differences to justify the use gamma-point sampling and "standard" potentials for the sake of computational efficiency.

To study the bulk liquid behavior of the quaternary hydride $Li_4BN_3H_{10}$ under a range of thermal conditions, we perform Born-Oppenheimer AIMD simulations at 600, 1000, and 2000 K using a canonical ensemble. In order to compare to the solid-state configuration, we also perform a simulation at 300 K. We choose the starting crystal structure as the 0 K relaxed 144 atom (8 f.u.) cubic periodic cell based on the work of Siegel *et al.*[8] which was based on the experimental structures from two groups.[5,6] In order to account for thermal expansion, we scale the 0 K relaxed supercell volume such that the average pressure is roughly zero at the target temperature.[36] However, we cannot know *a priori* if the simulations at 600 K and above will melt, providing us an indication of the liquid structure, or if they will remain solid. The latter case could occur for two reasons: (1) the simulation temperature is lower than the AIMD melting temperature or (2) the simulation temperature is above the AIMD melting point but the time scale for melting is longer than the simulation time. Thus, to briefly investigate the role of initial disorder, we use a volume-scaled version of the 2000 K final (i.e., melted) state as a second initial geometry at 600 K. In the figures that follow, we denote the results of this simulation as "600 K premelt."

We use a standard velocity-Verlet scheme with a time step of 0.5 fs for the time integration in our AIMD simulations.

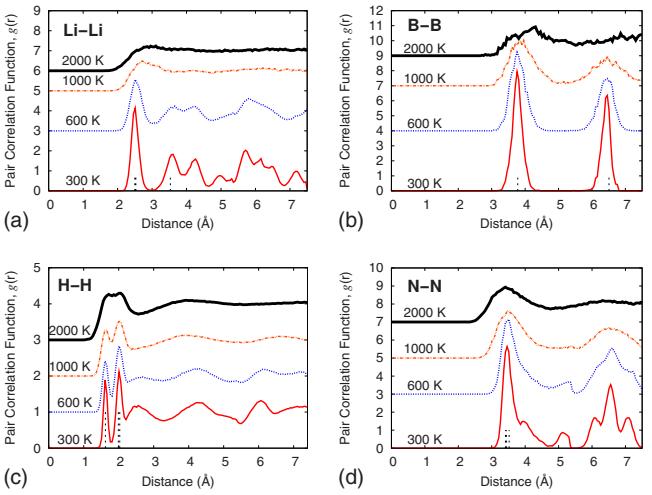

FIG. 1. (Color online) Pair-correlation functions, $g(r)$, versus distance for like atoms. Vertical dashed lines on the abscissa denote the position of the first three peaks in $g(r)$ for the 0 K relaxed structure. Curves have been offset for clarity.

Through testing, we found this time step to be sufficient to accurately capture H vibrations at the highest temperature without an excessive number of steps. We apply a Nose-type thermostat[37–39] to all the atoms in the system in order to simulate a canonical ensemble. We choose the mass parameter such that the frequency of the temperature fluctuations through a period of 250 fs corresponds to the average characteristic wave number for phonons in solid $Li_4BN_3H_{10}$ [$\sim$1000 cm^{-1} (Ref. 9)]. We allow the system to equilibrate for 1 ps (2000 time steps), then follow the system for an additional 4 ps (8000 time steps) to collect data for statistical analysis.

III. RESULTS AND DISCUSSION

A. Pair-correlation functions

To assess the local order of the $Li_4BN_3H_{10}$ system through the 300–2000 K temperature range, we calculate the time-averaged pair-correlation functions [i.e., $g(r)$ or radial distribution functions] for each pair of atom types. These functions give the probability of finding an atom of a given type at a given distance from a reference atom. We begin with a discussion of $g(r)$ for like-atom pairs.

The Li-Li pair-correlation functions [Fig. 1(a)] provide indications of significant structural changes between 600 and 1000 K. The pair-correlation function at 600 K has definite peaks similar to those in the solid-state 300 K case, indicative of structural ordering. The position of the peaks in the 300 and 600 K data correspond roughly to the separation distances of the Li^+ ions in the 0 K relaxed solid structure, though the decreasing prominence of the peaks with increasing temperature indicates greater disorder at higher temperatures. By 1000 K the distinct peaks have nearly disappeared, except a small peak at roughly 2.75 Å, corresponding to the nearest-neighbor distance in the 1000 K initial lattice structure. This nearest-neighbor peak is more broad than in the 600 K case, indicating a greater distribution of distances for

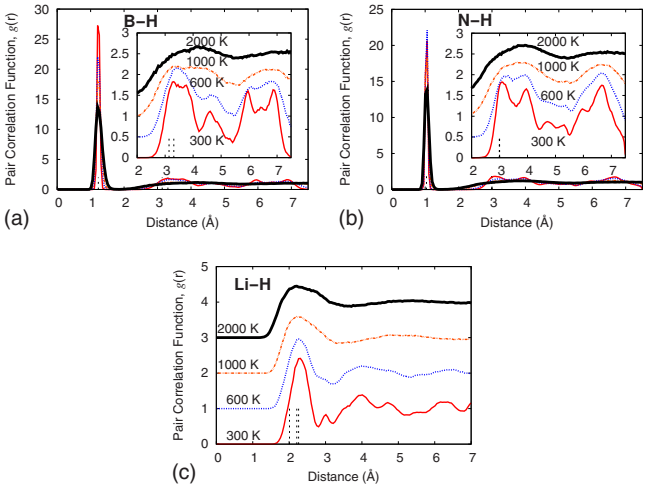

FIG. 2. (Color online) Pair-correlation functions, $g(r)$, versus distance for X-H atom type pairs. Vertical dashed lines on the abscissa denote the position of the first three peaks in $g(r)$ for the 0 K relaxed structure. Curves have been offset for clarity [only the 2.0–7.5 Å region for the B-H and N-H $g(r)$].

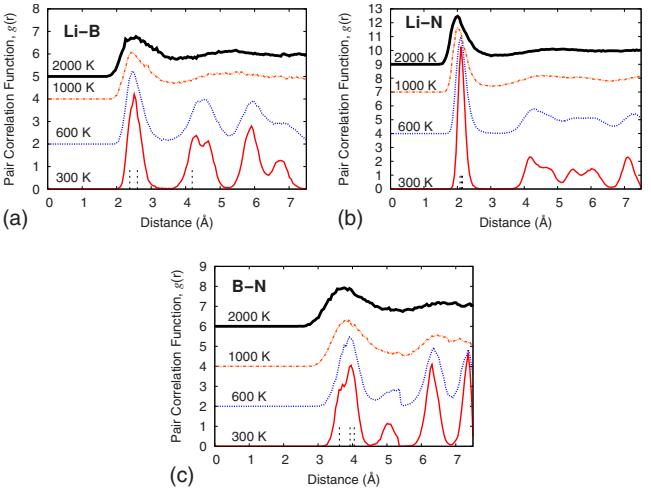

FIG. 3. (Color online) Pair-correlation functions, $g(r)$, versus distance for differing atom types (excluding X-H pairs). Vertical dashed lines on the abscissa denote the position of the first three peaks in $g(r)$ for the 0 K relaxed structure. Curves have been offset for clarity.

the nearest Li^+ ion. The lack of deep valleys in $g(r)$ at 1000 K indicates greater motion of the Li^+ ions. Meanwhile, at 2000 K, there are no significant peaks. This lack of clear maxima indicates that the Li^+ sublattice structure breakdown is nearly complete, approaching a uniform distribution beyond the first neighbor distance. Similarly, the H-H pair correlation shows a decrease in order as temperature increases, and a smoothing of the two major peaks at approximately 1.5 and 2 Å. This smoothing indicates a broader distribution of the H atoms in the system but still implies significant short-range order even at 2000 K. The behavior of the Li-Li and H-H pair correlations are in contrast to the B-B and N-N pair correlations [see Figs. 1(b) and 1(d)], which show strong pairwise structure well beyond the nearest-neighbor distance up to 1000 K. These results indicate the possibility of Li^+ sublattice melting[40] between 600 and 1000 K, where one sublattice in an ionic crystal becomes liquidlike while the others remain crystalline. Sublattice melting has been observed in Li_2NH (Ref. 28) and in a number of superionic conductors such as PbF_2,[41] BaF_2,[42] Li_xTiS_2,[43] Li_2SO_4,[44] and AgI.[45] Finally, by 2000 K the long-range order is gone from all sublattices and the system is fully liquidlike.

We next turn to $g(r)$ for unlike pairs of atoms. The B-H and N-H pair correlations for each temperature [see Figs. 2(a) and 2(b)] have a distinct nearest-neighbor peak, indicative of the presence of BH_4^- and NH_2^- anionic units at all temperatures. The initial peak indicates that the N-H and B-H bonds remain intact through the temperature range. An examination of the 2.0–7.5 Å sections of these figures [inset in Figs. 2(a) and 2(b)] shows that while there is oscillation about a value of $g(r)=1$ (relative to the offset in the figures) for distances greater than about 3 Å, the peaks are most pronounced in the 300 and 600 K cases. The shorter, more broad peaks at higher temperatures are characteristic of a decrease in order between B and H atoms in separate anionic units due to vibrational, rotational, or diffusive motion.

The Li-B and Li-N pair correlations [see Figs. 3(a) and 3(b)] give information about the correlation between the cations and anions within the system while the B-N pair correlations [see Fig. 3(c)] indicates ordering between the BH_4^- and NH_2^- anionic units. The trends in the pair correlations with temperature are qualitatively similar to the Li-Li pair-correlation function with one important distinction. In the Li-B, Li-N, and B-N cases, even at 2000 K, there is still a correlation peak at roughly the nearest-neighbor range followed by a shallow valley, which indicates a short-range correlation between the cations and anions remains at all temperatures.

B. Bond-angle distributions

The strong peaks in our B-H and N-H pair correlations [Figs. 2(a) and 2(b)] indicate the existence of BH_4^- and NH_2^- anionic units through the entire temperature range. To further investigate the structure of the anionic units, we examine the H-B-H and H-N-H bond-angle distributions [see Figs. 4(a) and 4(b)]. If the anionic units were perfectly rigid, the angle distributions would have a sharp peak at the angle corresponding to the bond angle in the rigid anionic unit. Thus, the width of our angle distributions is an indication of the extent to which these units are nonrigid.

We find a very wide range of angles in both anionic units (full width at half maximum: ~10° at 300 K, ~30° at 2000

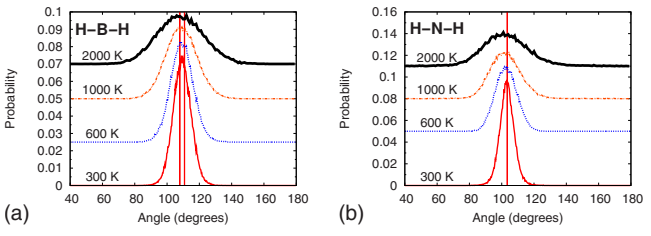

FIG. 4. (Color online) H-B-H and H-N-H angle distributions for the temperatures studied, with the 0 K relaxed solid values as reported in Ref. 8 (vertical lines) for reference.

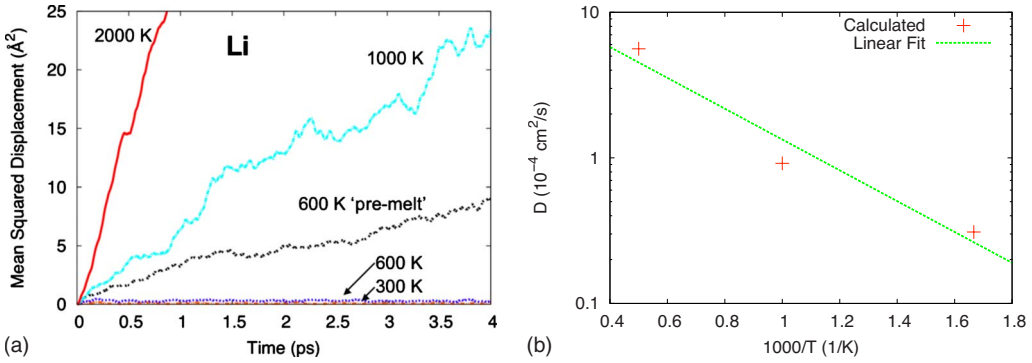

FIG. 5. (Color online) (a) Li^+ mean-squared displacement. (b) Arrhenius plot of the Li^+ diffusivity using 600 K premelt case (the rightmost point). The diffusivity for the 600 K case is too low to appear in (b). The activation energy (Q) and pre-exponential factor (D_0) for Li^+ diffusion were calculated to be 20 kJ/mol and 15×10^{-4} cm^2/s, respectively.

K). Of particular note is that even at 300 K, we no longer see the two distinct H-B-H angles found in the relaxed solid. Further, at all temperatures, the mean H-B-H angle is less than the ideal tetrahedral angle (109.5°) that would exist in a perfectly rigid, ideal BH_4^- units. Thus, while the pair correlations indicate that the NH_2^- and BH_4^- units remain intact, they are certainly not simple rigid units, as the angular distributions suggest. Specifically, the anionic units undergo significant deformation even before the onset of Li sublattice melting.

C. Mean-squared displacement and diffusivity

In addition to the equilibrated structural information above, we can examine the diffusive motion of each species during the simulations. At each temperature, we calculate the mean-squared displacement (MSD) of each atom type as a function of time. From the slope of a linear fit to the MSD data versus time we estimate the diffusivity, $D=D_0e^{Q/kT}$, of each species. The MSD for Li^+ [Fig. 5(a)] yields a diffusivity that exhibits an approximately Arrhenius behavior [see Fig. 5(b)] through the temperature range studied. However, in the 600 K case, the flat MSD curve indicates very little diffusion or disordering of the Li^+ cations during the time studied. The lack of Li^+ cation disordering is in agreement with the Li-Li pair correlation at 600 K. In contrast, we find the Li^+ MSD and diffusivity of the 600 K "premelt" case to be significantly larger and more liquidlike. Based on our 600 K premelt, 1000 and 2000 K data, we estimate a very high Li^+ diffusivity with an activation energy, Q, of approximately 20 kJ/mol and a pre-exponential factor, D_0, of approximately 15×10^{-4} cm^2/s. This activation barrier is roughly three times larger than the Li^+ diffusion activation energy reported in Li_2NH,[28] but our values are still in the range of other Li^+ superionic conductors.[43,44]

The near-zero diffusivity of the 600 K case and nonzero diffusivity of the 600 K premelt case point to metastability of the solid and/or liquid phases at 600 K. Specifically, at 600 K, the system tends to stay in the same state that it starts. For the premelted (i.e., liquid initial state) case this means the system remains a liquid, either because 600 K is above the DFT melting temperature or the time scale is too short for the system to freeze. Conversely, for the solid initial state, 600 K is either below the DFT melting temperature or the time scale is too short for the system to melt. Considerations such as these make a quantitative determination of the melting point from our AIMD calculations difficult.

The B, N, and H MSDs [see Figs. 6(a)–6(c)], indicate that there is no significant diffusion of B, N, or H up to 1000 K while at 2000 K there is significant diffusion of both species. At 1000 K and below, we see MSD "saturation:" an initially increasing MSD which finally oscillates about some constant value. The initial rise of the MSD is especially noticeable in the H MSD at 1000 K. This behavior is consistent with vibrational and rotational motion of the anionic units with respect to nominally fixed lattice sites, and thus signifies some measure of crystalline structure in some sublattices over the time scale studied [see Fig. 7]. We find the 2000 K diffusivity for B, N, and H to be approximately 1×10^{-4}, 1.5×10^{-4}, and 1.5×10^{-4} cm^2/s, respectively, approximately four times smaller than the Li^+ diffusivity of roughly 5×10^{-4} cm^2/s.

To gain a more intuitive picture of the structural changes in structure as a function of temperature, we produced the cumulative trajectory plot in Fig. 7. This figure shows the trajectory of each N, B, and Li atom through the postequilibration period as a series of lines, projected onto the (100) plane. In this way, we can easily visualize how localized the atoms remain through the simulation time. For example, at 300 K, the lines for each atom are strongly localized on a lattice, indicating a vibrating but crystalline solid. Meanwhile, the 2000 K image shows the trajectories crossing one another with no discernible structure, indicative of a liquid. Of more interest are the three frames at intermediate temperatures. The two 600 K cases show clearly how the initial disorder of the 600 K "premelted" state allows for greater mobility of the Li atoms, while the B and N remain much more localized, but all of the sublattices are less localized than the 600 K case. Additionally, the 1000 K case makes it more clear that the Li sublattice is diffuse while the other lattices remain localized in further support of our earlier conclusion of Li^+ sublattice melting at a temperature below 1000 K.

D. Velocity autocorrelation function power spectrum

Next, we turn to the vibrational behavior of $Li_4BN_3H_{10}$. To address this, we calculate the power spectrum of the ve-

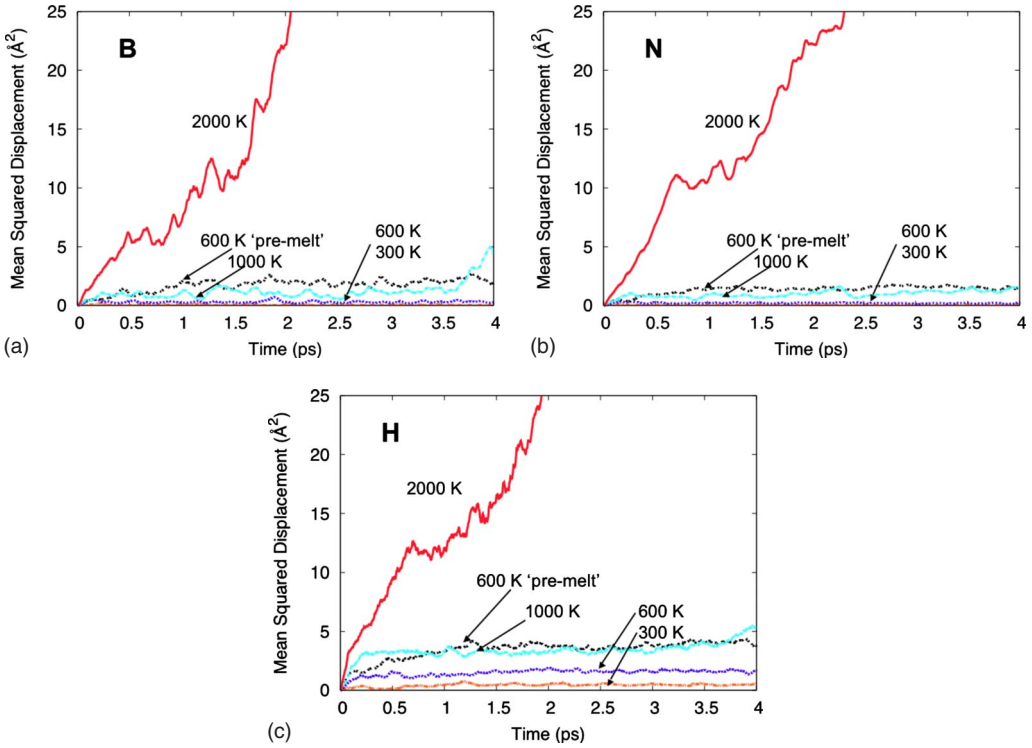

FIG. 6. (Color online) Mean-squared displacements of B, N, and H versus time for the temperatures studied. We calculated the Li^+ diffusivity at 2000 K to be approximately four times larger than that of these species. Calculation of D at 2000 K is based on the slope of the MSD, however due to the behavior at temperatures below 2000 K D could not be accurately computed for the B, N, and H species at the lower temperatures. As a result, D_0 and Q could not be computed for these species.

locity autocorrelation function (VAF). This quantity provides us with a measure of vibrational frequencies, that is, analogous to the phonon spectra in the solid.[46,47] The VAF is defined as follows:

$$\mathrm{VAF}(t) = \frac{1}{N}\sum_{i=1}^{N} [\mathbf{v}_i(t_0) \cdot \mathbf{v}_i(t)], \tag{1}$$

where $\mathbf{v}_i(t)$ is the velocity of atom i at time t. Here, N indicates the total number of atoms in the system and we chose t_0 to correspond to the beginning of the time-averaging window described earlier. The power spectrum is then defined as the absolute square of the Fourier transform of the VAF. To smooth out the numerical noise from the discrete Fourier transform prior to plotting, we applied a Gaussian smoothing operation to each of the data points using a mean of 0 (i.e., centered on the data point to be smoothed), a standard deviation of 1.0 data point ($\sim$8.34 cm^{-1}) and a window of ± 5 data points ($\sim$41.7 cm^{-1}). For convenience, we normalized the VAF power spectrum at each temperature such that its integral was equal to 1.0.

We find that the frequencies of the major peaks remain roughly the same at all temperatures, indicating little change in the vibrations and therefore the ionic units present in the system [see Fig. 8]. This result agrees with our structural and diffusion findings. In the 600 K case, the largest peak is at roughly 3300 cm^{-1}, much like the 300 K solid $Li_4BN_3H_{10}$ case. This frequency matches well with the N-H stretching modes in the NH_2^- anionic units based on DFT calculations of the optical-phonon modes in $LiNH_2$ by Miwa *et al.*[19] We also find a set of peaks at 2300–2500 cm^{-1}, which are close to the set of three peaks at roughly 2200–2300 cm^{-1} that Racu *et al.*[48] attribute to the BH_4^- stretching modes in $LiBH_4$ and Chater *et al.*[6] indicate that this mode in $Li_4BN_3H_{10}$ is in approximately the same range. The set of peaks between 1000 and 1600 cm^{-1}, which Wu *et al.*[9] attribute to the symmetric and asymmetric H-N-H and H-B-H bond deformation modes in $Li_4BN_3H_{10}$.

In the 300 and 600 K cases we find 100–800 cm^{-1} peaks, which[9] attributes to low-frequency Li^+, NH_2^-, and BH_4^- vibrations and rotations. These 100–800 cm^{-1} peaks are significantly smaller than the $\sim$3000 cm^{-1} peak, indicating that higher frequency "internal" vibrational modes (vibrations within anionic units) dominate at low temperature as one would expect in a crystalline solid. This is contrary to the 1000 and 2000 K cases where the largest peak is closer to about 300–400 cm^{-1} with the $\sim$3300 cm^{-1} peak becoming less prominent. We find the decrease in prominence of the high-frequency modes relative to the low-frequency modes with increasing temperature to agree well with the onset of liquidlike behavior. This shift in the prominent modes may be explained by the breakdown in the crystal structure, which would allow low-frequency vibrations and rotations to occur more freely than in the solid. We have provided a summary of the major vibrational frequencies, including the corresponding phenomena from several authors in Table I.

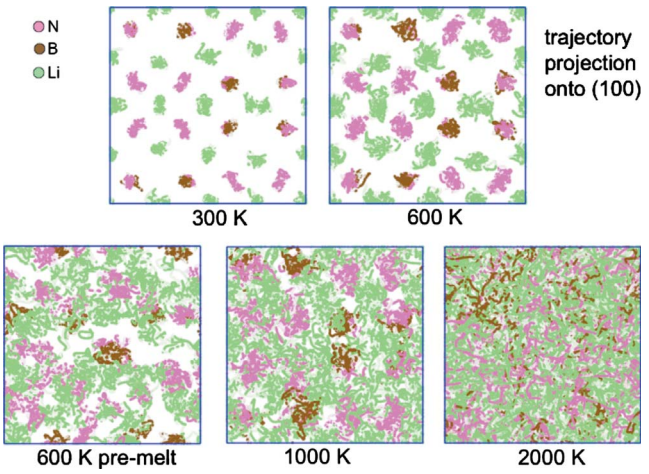

FIG. 7. (Color online) Projection of B (brown), N (pink), and Li (green) trajectories onto (100) for the postequilibration period. These figures illustrate the Li^+ sublattice melting phenomenon indicated by the like-atom pair correlations in Figs. 1(a)–1(d) as well as the MSD saturation effect in Figs. 6(a) and 6(b). The N and B atoms trajectories are noticeably localized up to 1000 K while the Li atoms clearly diffuse through the structure at the same temperature. At 2000 K all species are diffusing with no discernible crystal lattice.

E. Ammonia formation in bulk liquid

The previous analyses all pointed toward the bulk liquid behaving as a mixture of Li^+, BH_4^-, and NH_2^-, where the BH_4^- and NH_2^- remained intact. We verified this with a Bader charge analysis[49] using the program "BADER"[50–52] and our AIMD data. We found no widespread changes in the atomic partial charges of the liquid compared to the solid. However, we find localized chemical fluctuations of the anionic units and evidence of hydrogen transfer between units. Close examination of the atomic trajectories and partial charges through the simulation, including the thermal equilibration period (i.e., prior to collecting the data used in the previous sections) reveals the formation of a single NH_3 molecule in the 1000 and 2000 K cases via the reaction of two amide anions to form an ammonia molecule and an imide anion: $2NH_2^- \rightarrow NH_3 + NH^{2-}$ [see Fig. 9]. This NH_3 molecule remains stable for the duration of the 1000 K simulation. In the 2000 K case, two NH_2^- units react to form $NH_3 + NH^{2-}$ as in the 1000 K case; after the reaction, these molecules moved away from one another over a period of roughly 50 fs. During this time, the NH^{2-} interacts with a third NH_2^- unit and one H atom is transferred to the NH^{2-} ion, i.e., $NH_2^- + NH^{2-} \rightarrow NH^{2-} + NH_2^-$. A similar hydrogen transfer process is repeated once again roughly 2.4 ps later. Because the majority of BH_4^- and NH_2^- units at 1000 and 2000 K remained intact, it is difficult to detect this reaction based only on the quantities discussed in the previous sections. In situations like these, the fine spatial and temporal resolution of AIMD can be extremely helpful to fully understanding a system and finding chemical reactions.

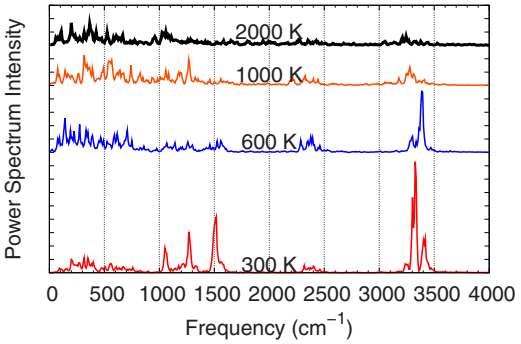

FIG. 8. (Color online) Power spectrum of the velocity autocorrelation function for the temperatures studied. Each temperature has been offset such that there is no overlap in the data and normalized so that the integral in time is equal to one.

IV. CONCLUSIONS

We performed canonical (NVT) AIMD calculations of bulk $Li_4BN_3H_{10}$ at four temperatures, from roughly half to four times the experimental melting temperature, to provide insight into the nature of the liquid phase. We characterized the structure at each temperature using pair-correlation functions and angle distributions for each species. In order to assess the diffusivity and vibrational behavior, we calculated the mean-squared displacements for each atom type and the

TABLE I. Summary of phonon frequency data of the solid from several authors based on experimental measurements and DFT calculations for comparison to our AIMD data in Fig. 8.

Frequencies (cm^{-1})	Corresponding phenomenon	Experiment or DFT	Material
400–500	NH_2^- and BH_4^- unit libration	Experiment and DFT[a]	$Li_4BN_3H_{10}$
600–700	H-N-H bond bending	Experiment and DFT[a]	$Li_4BN_3H_{10}$
1000–1300	H-B-H bending, asymmetric stretching	Experiment and DFT[a]	$Li_4BN_3H_{10}$
1400–1500	N-H asymmetric stretching	Experiment and DFT[a]	$Li_4BN_3H_{10}$
~2300	BH_4^- symmetric stretching	Experiment	$LiBH_4$ [b] and $Li_4BN_3H_{10}$ [c]
~3300	NH_2^- symmetric stretching	Experiment and DFT	$LiNH_2$ [d] and $Li_4BN_3H_{10}$ [c]

[a]Reference 9.
[b]Reference 48.
[c]Reference 6.
[d]Reference 19.

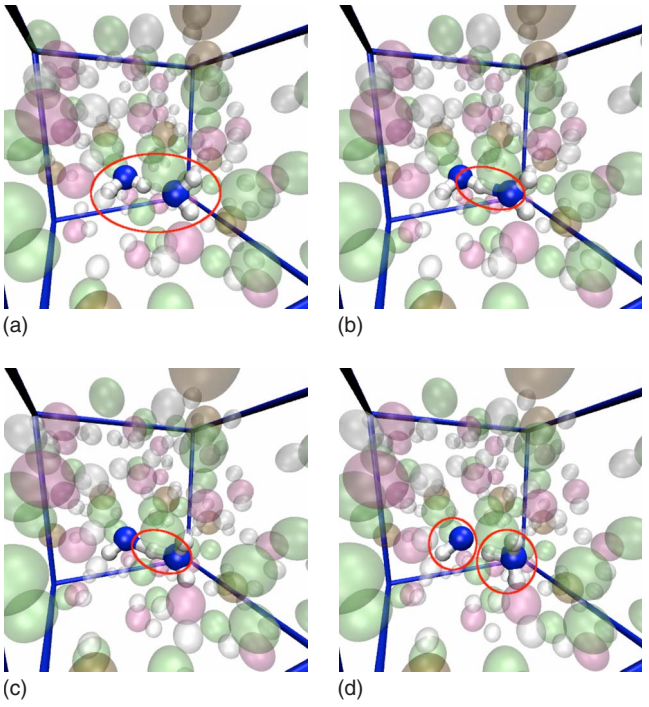

FIG. 9. (Color online) Snapshots of NH_3+NH^{2-} formation at 1000 K during the thermal equilibration phase. (a) Two neighboring NH_2^- units approach one another, (b) allowing an N and an H atom to get close enough for the H and N atoms to form a bond, though the H is still more closely bound to the left-hand N atom, and (c) finally forms an arrangement where the H atom is closer to the right-hand N atom, though the bonds are still in a relatively planar arrangement (c), finally leading to stable NH_3 (with nonplanar bonds) and NH^{2-} in (d). The total simulated time passing in this process is roughly 10 fs.

power spectrum of the velocity autocorrelation function for the entire system.

Our analysis of the structure yielded several insights. We found evidence that the Li^+ sublattice structure broke down prior to the other sublattices, suggesting the possibility of Li^+ sublattice melting in this material. Our study indicated that the BH_4^- and NH_2^- units remained intact but undergo surprisingly large deformations. We also found that there were indications of significant order between Li^+ and BH_4^-, Li^+ and NH_2^- as well as BH_4^- and NH_2^-. This combined with a Bader charge analysis led us to the conclusion that the liquid structure, like the solid, is best described as a mixture of Li^+, BH_4^-, and NH_2^- units with ionic interactions between them. Despite indications that the anionic complexes remained intact based on time and spatial averaged data, we found the bond-breaking reaction $2NH_2^- \rightarrow NH_3+NH^{2-}$ occurred during thermal equilibration at 1000 and 2000 K.

From the structural and dynamic behavior, we were able to discern that our system at 600 K is metastable with respect to melting. The diffusivity study revealed that the Li^+ diffusivity and activation energy was in the range of several Li^+ superionic conductors. The small diffusivity of the non-Li species at the lower end of the temperature range indicated that $Li_4BN_3H_{10}$ may have a long time scale for disordering. However, more work is needed to fully address this question. Finally, we were able to find that each temperature showed similar characteristic vibrational frequencies to the solid. Comparison to published phonon frequencies indicates that the BH_4^- and NH_2^- symmetric stretching modes decreased in prominence with increasing temperature while the low-frequency rotational and vibration modes increased in prominence.

ACKNOWLEDGMENTS

We would like to thank Bryce Meredig, Alex Thompson, Daniel Shapiro, Don Siegel, Andrea Sudik and Bill Schneider for their input during this work. This work was supported by DOE under Grant No. DE-FG02-07ER46433. This research was supported in part by the National Science Foundation through TeraGrid resources. The computations were performed in part on the Kraken system at the National Institute for Computational Sciences.

*davidfarrell2008@u.northwestern.edu
†c-wolverton@northwestern.edu

[1] S. Satyapal, J. Petrovic, C. Read, G. Thomas, and G. Ordaz, Catal. Today **120**, 246 (2007).
[2] *Hydrogen in Metals II, Application-Oriented Properties*, Topics in Applied Physics Vol. 29, edited by G. Alefeld and J. Völkl (Springer-Verlag, Berlin, 1978).
[3] S. Orimo, Y. Nakamori, J. Eliseo, A. Züttel, and C. Jensen, Chem. Rev. (Washington, D.C.) **107**, 4111 (2007).
[4] F. Pinkerton, G. Meisner, M. S. Meyer, M. Balogh, and M. Kundrat, J. Phys. Chem. B **109**, 6 (2005).
[5] Y. Filinchuk, K. Yvon, G. Meisner, F. Pinkerton, and M. Balogh, Inorg. Chem. **45**, 1433 (2006).
[6] P. Chater, W. David, S. Johnson, P. Edwards, and P. Anderson, Chem. Commun. (Cambridge) **23**, 2439 (2006).
[7] J. Herbst and L. Hector, Jr., Appl. Phys. Lett. **88**, 231904 (2006).
[8] D. J. Siegel, C. Wolverton, and V. Ozoliņš, Phys. Rev. B **75**, 014101 (2007).
[9] H. Wu, W. Zhou, T. Udovic, J. Rush, and T. Yildirim, Chem. Mater. **20**, 1245 (2008).
[10] F. Pinkerton and M. Meyer, J. Phys. Chem. C **113**, 11172 (2009).
[11] C. Wolverton, V. Ozoliņš, and M. Asta, Phys. Rev. B **69**, 144109 (2004).
[12] A. R. Akbarzadeh, V. Ozoliņš, and C. Wolverton, Adv. Mater. (Weinheim, Ger.) **19**, 3233 (2007).
[13] S. Alapati, J. Johnson, and D. Sholl, Phys. Chem. Chem. Phys. **9**, 1438 (2007).
[14] C. Wolverton, D. Siegel, A. Akbarzadeh, and V. Ozoliņš, J. Phys.: Condens. Matter **20**, 064228 (2008).
[15] V. Ozoliņš, E. Majzoub, and C. Wolverton, Phys. Rev. Lett. **100**, 135501 (2008).

[16] S. Shevlin and Z. Guo, Chem. Soc. Rev. **38**, 211 (2009).
[17] Z. Łodziana and T. Vegge, Phys. Rev. Lett. **93**, 145501 (2004).
[18] E. Majzoub, K. McCarty, and V. Ozoliņš, Phys. Rev. B **71**, 024118 (2005).
[19] K. Miwa, N. Ohba, S. Towata, Y. Nakamori, and S. Orimo, Phys. Rev. B **71**, 195109 (2005).
[20] B. Magyari-Köpe, V. Ozoliņš, and C. Wolverton, Phys. Rev. B **73**, 220101 (2006).
[21] T. Mueller and G. Ceder, Phys. Rev. B **74**, 134104 (2006).
[22] C. Wolverton and V. Ozoliņš, Phys. Rev. B **75**, 064101 (2007).
[23] Z. Ma and M. Chou, J. Appl. Phys. **104**, 093619 (2008).
[24] Y. Lee, Y. Kim, Y. Cho, D. Shapiro, C. Wolverton, and V. Ozoliņš, Phys. Rev. B **79**, 104107 (2009).
[25] H. Gunaydin, K. Houk, and V. Ozoliņš, Proc. Natl. Acad. Sci. U.S.A. **105**, 3673 (2008).
[26] H. Lee, D. Kim, N. Singh, M. Kołaski, and K. Kim, J. Chem. Phys. **127**, 164311 (2007).
[27] N. Zarkevich and D. Johnson, Phys. Rev. Lett. **100**, 040602 (2008).
[28] C. Araújo, A. Blomqvist, R. Scheicher, P. Chen, and R. Ahuja, Phys. Rev. B **79**, 172101 (2009).
[29] G. Kresse and J. Hafner, Phys. Rev. B **47**, 558 (1993).
[30] G. Kresse and J. Hafner, Phys. Rev. B **49**, 14251 (1994).
[31] G. Kresse and J. Furthmüller, Comput. Mater. Sci. **6**, 15 (1996).
[32] G. Kresse and J. Furthmüller, Phys. Rev. B **54**, 11169 (1996).
[33] G. Kresse and D. Joubert, Phys. Rev. B **59**, 1758 (1999).
[34] J. Perdew and Y. Wang, Phys. Rev. B **45**, 13244 (1992).
[35] P. Blöchl, Phys. Rev. B **50**, 17953 (1994).
[36] The pressure for each temperature was determined by scaling the supercell to a known value and running the simulation for 500 time steps. We repeated this process until a supercell size was found where the pressure fluctuated near zero.
[37] S. Nose, J. Chem. Phys. **81**, 511 (1984).
[38] S. Nose, Prog. Theor. Phys. Suppl. **103**, 1 (1991).
[39] D. Bylander and L. Kleinman, Phys. Rev. B **46**, 9837 (1992).
[40] W. Hayes, Contemp. Phys. **27**, 519 (1986).
[41] J. Boyce, J. Mikkelsen, Jr., and M. O'Keeffe, Solid State Commun. **21**, 955 (1977).
[42] A. Ivanov-Shitz, A. Buchstab, S. Aityan, and H.-H. Kohler, Appl. Phys. A **54**, 251 (1992).
[43] R. Winter and P. Heitjans, J. Phys. Chem. B **105**, 6108 (2001).
[44] R. Tärneberg and A. Lundèn, Solid State Ionics **90**, 209 (1996).
[45] M. Delaney and S. Ushioda, Phys. Rev. B **16**, 1410 (1977).
[46] N. March and M. Tosi, *Introduction to Liquid State Physics* (World Scientific, Singapore, 2002).
[47] N. March and M. Tosi, *Atomic Dynamics in Liquids* (Dover, New York, 1976).
[48] A.-M. Racu, J. Schoenes, Z. Lodziana, A. Borgschulte, and A. Züttel, J. Phys. Chem. A **112**, 9716 (2008).
[49] R. Bader, *Atoms in Molecules, a Quantum Theory* (Oxford Science, Oxford, London, 1990).
[50] G. Henkelman, A. Arnaldsson, and H. Jónsson, Comput. Mater. Sci. **36**, 354 (2006).
[51] E. Sanville, S. Kenny, R. Smith, and G. Henkelman, J. Comput. Chem. **28**, 899 (2007).
[52] W. Tang, E. Sanville, and G. Henkelman, J. Phys.: Condens. Matter **21**, 084204 (2009).